Geophys. J. R. astr. Soc. (1982) **68**, 371–388

On the electrical crust–mantle structure in Fennoscandia: no Moho, and the asthenosphere revealed?

Alan G. Jones *Institut für Geophysik der Westfälischen Wilhelms-Universität, Corrensstrasse 24, D-4400 Münster, Federal Republic of Germany*

Received 1981 May 12; in original form 1981 March 3

Summary. An interpretation of the geomagnetic inductive response function, $C(\omega, 0)$, observed at Kiruna in northern Sweden, is herein undertaken. The bounds of acceptable solutions are initially discovered by a Monte-Carlo random search procedure, and the best-fitting solutions are examined by the application of linear theory to the problem. The data are shown to have a higher degree of internal consistency than that described by the estimated variances of each datum. A further Monte-Carlo inversion of the variance-reduced data set gives solutions with well defined model parameters.

The two major features of the models are: (1) a small, or non-existent, electrical conductivity variation across the seismic Moho boundary, and (2) the unequivocal existence of an electrical asthenosphere, under the Fenno-scandian shield, beginning at a depth of between 155–185 km, and of 60 km minimum thickness. Both of these observations have seismic counterparts.

Finally, possible mantle temperature profiles are deduced which depend on the assumptions and laboratory data employed.

1 Introduction

The electrical crust–mantle structure of the continents and oceans may play a decisive role in helping to understand the tectonic processes that have occurred, or are, at present, occurring. Knowledge of the electrical resistivity with depth structure beneath a measuring point may lead to an interpretation of, for example, the probable conditions at certain depths, the possible rock candidates responsible for the observations, and a mantle geotherm for the region etc. These factors are all of significant importance when attempting to build a suitable tectonic model of a region, and the interaction between the region and the other environments with which it is juxtaposed.

However, the geomagnetic induction worker has, at his disposal, some response function describing the variation of the observations with frequency, which he desires to interpret into a conductivity model believed to be responsible for the observations. But modelling of data may suffer from the effects of bias due to either oversimplification, or overcomplication, of the problem, or simply lack of sufficient information. Another point of extreme

Downloaded from https://academic.oup.com/gji/article/68/2/371/692185 by guest on 20 April 2024

relevance is: how valid are the assumptions that are made when deriving a model, or models, from data.

This latter point was dealt with, for the data set under consideration, in a previous publication (Jones 1980), in which it was shown conclusively that an interpretation of the data in terms of a model where conductivity varies with depth alone is fully justifiable. Part of this work addresses the first point detailed above.

The first part of the paper, Section 2, describes how acceptable models were discovered utilizing a refined version of Jones & Hutton's (1979) Monte-Carlo inversion procedure. In the second part, Section 3, the best-fitting 3- and 4-layer solutions discovered are examined, by application of a singular value decomposition (SVD) of the system matrix, for parameter resolution and parameter intercorrelation. The importance of *a priori* information is illustrated. The third part, Section 4, correlates the geoelectric model for the border regions of Fennoscandia with seismic models of the region, whilst the final part, Section 5, proposes a tentative mantle geotherm for the Fennoscandian shield.

2 Data and models

The data with which this paper is concerned were derived by applying the Horizontal Spatial Gradient (HSG) method (Schmucker 1970) to various time segments, or 'events', recorded by ten magnetometers located at, and around, Kiruna in northern Sweden (Jones 1980). These events were principally analysed as part of the International Magnetospheric Study (IMS), to which Münster University contributed by operating an array of 36 modified Gough-Reitzel variometers (Gough & Reitzel 1967; Küppers & Post 1981). However, the large gradients observed in the horizontal magnetic fields made these events also suitable for geomagnetic induction studies.

The application of the HSG technique to the 3-component magnetic variations yielded an estimate of the complex inductive transfer function, $\hat{C}(\omega, 0)$ (Schmucker 1970; Schmucker & Weidelt 1975), in the period range 10^2–10^4 s. The estimate was shown to be physically realizable, i.e. causal, by two techniques, one involving the Fourier transformation of the complex conjugate of $\hat{C}(\omega, 0)$, i.e. $\hat{C}^*(\omega, 0)$, and the other entailing the Hilbert transformation of the real part of $\hat{C}(\omega, 0)$. (It cannot be stressed too highly that causality is a *necessary condition* of all transfer functions, and the simple tests outlined in Jones (1980), or some equivalent ones, should be much more widely applied in all branches of geophysics.) The estimate was also displayed to be interpretable in terms of an earth conductivity model in which the electrical conductivity varies with depth alone, $\sigma(z)$, by applying validity tests both in the frequency domain (Weidelt 1972) and time domain (Weidelt, private communication, detailed in Jones 1980).

The inductive transfer function, $C(\omega, k)$, is representable as magnetotelluric (MT) apparent resistivity, ρ_a, and phase, ϕ, reponses by the relationships

$$\rho_a(\omega, k) = \omega\mu_0 |C(\omega, k)|^2$$

$$\phi(\omega, k) = -\tan^{-1}\left(\frac{\text{Re}\,[C(\omega, k)]}{\text{Im}\,[C(\omega, k)]}\right)$$

where ω is the frequency of interest, and k is the Price wavenumber (Price 1962) of the source.

The thus determined $\rho_a(T)$ and $\phi(T)$ (henceforth a uniform external field is assumed, i.e. $k = 0$), together with their 80 per cent confidence intervals, derived as described in Jones (1980), are illustrated in Fig. 1.

These data were inverted to acceptable geoelectric models by a refined version of the

Downloaded from https://academic.oup.com/gji/article/68/2/371/692185 by guest on 20 April 2024

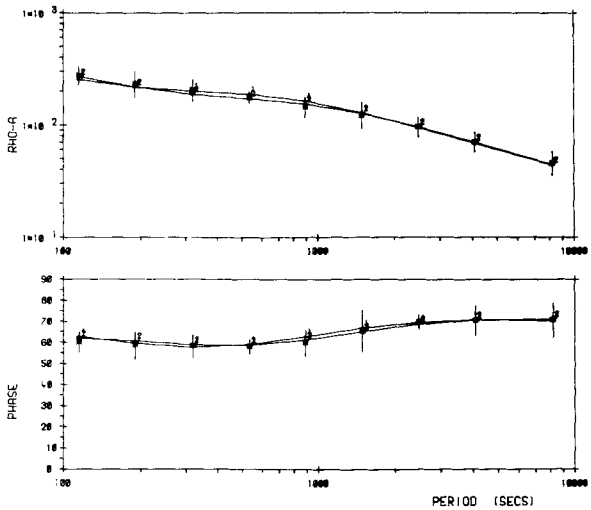

Figure 1. The fit of the best 3-layer (numbered '1') and best 4-layer (numbered '2') models (detailed in Table 1) to the derived inductive response function, expressed in terms of apparent resistivity and phase, with 80 per cent confidence intervals as shown.

Monte-Carlo technique (Jones 1977; Jones & Hutton 1979) with the assumptions of a three-layered earth, and that the top layer had a resistivity of $10^4\Omega$m. This latter constraint was taken from the audiomagnetotelluric observations of Westerlund (1972) made in the vicinity of Kiruna, and the former from the essential nature of the derived response. As discussed in Jones & Hutton (1979), it is *axiomatic* in geophysical data interpretation to find the simplest model – or models – that satisfies the observed response, unless any *a priori* information is available. In this respect, three-layer geoelectric models can be found that well describe the data. Hence, the first inversion was undertaken with one constant, i.e. $\rho_1 = 10^4\,\Omega$m, and four variables, ρ_2, ρ_3, h_1 and h_2, i.e. the resistivities of the second and third layers, and the thickness of the first and second layers. The four variables were only constrained to be physically reasonable, i.e. $1\,\Omega\text{m} < \rho_2$ and $\rho_3 < 10^5\,\Omega$m and $0 < h_1$ and h_2. The refined version of the Monte-Carlo search procedure operates initially as that described in Jones & Hutton (1979), but restricts the search space of the random choice of parameters once a certain minimum number of models have been found. Hence, it can be regarded as similar to the Hedgehog procedure (Keilis-Borok & Yanovskaya 1967), with the important difference that degeneracy of the solution space is permitted, i.e. a single closed set of solutions is not an essential pre-requisite of the data and globally distinct solutions are discovered.

Using the procedure with the starting model as given in Jones (1980), $\rho_1 = 10^4\,\Omega$m, $\rho_2 = 125\,\Omega$m, $\rho_3 = 3\,\Omega$m, $h_1 = 30$ km and $h_2 = 110$ km, those models discovered, out of 6000 tested, which were acceptable to all 18 confidence intervals (nine for ρ_a and nine for ϕ), had ρ–d (resistivity–depth) profiles as shown in Fig. 2. The best fitting model, and the standard deviations of the acceptable values of each of the parameters, are listed in Table 1, and the theoretical response of this best model is illustrated in Fig. 1. As can be seen in Fig. 2, $\log(\rho_2)$, the logarithm of the second layer, is the best estimated parameter from the data set, and h_2 the worst estimated.

For reasons which will be discussed in Section 4, a second Monte-Carlo inversion of the data set was undertaken with the assumptions of a four-layered earth, $\rho_1 = 10^4\,\Omega$m (as previous) and $h_1 + h_2 = 46$ km, i.e. the depth to the interface between the second and third

Downloaded from https://academic.oup.com/gji/article/68/2/371/692185 by guest on 20 April 2024

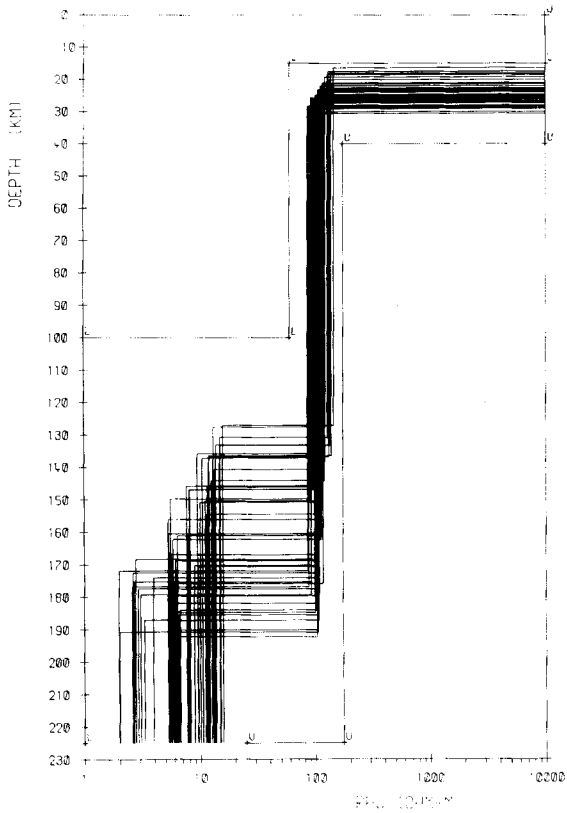

Figure 2. The resistivity–depth profiles of those 3-layer models, discovered by the Monte-Carlo random search procedure, that are acceptable to all 18 80 per cent confidence intervals of the data, as illustrated in Fig. 1. The final bounds of the search procedure are indicated by the ρ–d profiles marked L for lower bound, and U for upper bound.

layers. Thus, there were five variables, ρ_2, ρ_3, ρ_4, h_1–h_2 and h_3. Of the 6000 models investigated, those that were acceptable to all 18 confidence intervals had ρ–d profiles as illustrated in Fig. 3. The best fitting 4-layer model discovered is detailed in Table 1, as are the standard deviations of the accepted values of the model parameters, and its theoretical response is shown in Fig. 1.

3 Model parameter correlations and reliability

3.1 THEORY

In inversion studies, it is of paramount importance to discover four features described by the data set under consideration. These are: (1) the 'best' (defined in some manner) fitting solution; (2) the degree of non-uniqueness of that solution; (3) the correlation between the model parameters of that solution; and (4) the ability of the data to resolve the model parameters of that solution, i.e. in essence the reliability of the derived model parameters. It is obvious that (4) is intimately connected to (2). Unfortunately, in the majority of geophysical interpretations of data, only (1) is attempted.

Points (1) and (2) have been covered in the previous section where best-fitting (as defined by a minimum value of ψ given by equation (1) of Jones & Hutton 1979) 3- and 4-layer

Downloaded from https://academic.oup.com/gji/article/68/2/371/692185 by guest on 20 April 2024

Table 1. Parameters of the best fitting 3- and 4-layer models to the data illustrated in Fig. 1. Figures in brackets refer to ± 1 standard deviation from the means of the acceptable model parameters, where a logarithmic parameter distribution has been assumed, i.e. 68 per cent of acceptable parameters were within the bounds specified in brackets.

	Crust	Mantle	Asthenosphere
	One layer		
3-layer model	$\rho = 10^4$ Ωm (fixed) h = 27.3 km (22.3–28.6) d = as h	ρ = 103 Ωm (92.7–113.6) h = 133.7 km (123.3–153.5) d = 161.0 km (147.6–180.0)	ρ = 6.4 Ωm (2.9–9.6)
	Two layers		
4-layer model	$\rho_1 = 10^4$ Ωm (fixed) h_1 = 7.1 km (5.0–11.8) d_1 = as h_1	ρ = 77 Ωm (72.1–91.6) h = 127 km (111.3–143.2) d = 173 km (157.5–189.0)	ρ = 5.1 Ωm (2.3–7.8)
	ρ_2 = 360 Ωm (240–450) h_2 = 38.9 km (33.0–42.1) d_2 = 46 km (fixed)		

models were discovered (detailed in Table 1), and their non-uniquenesses displayed (Figs 2 and 3). To accomplish points (3) and (4), certain aspects of linear theory have been employed here. For a more complete exposition of the following theory, the reader is referred to, for example, Wiggins (1972) and Inman (1975).

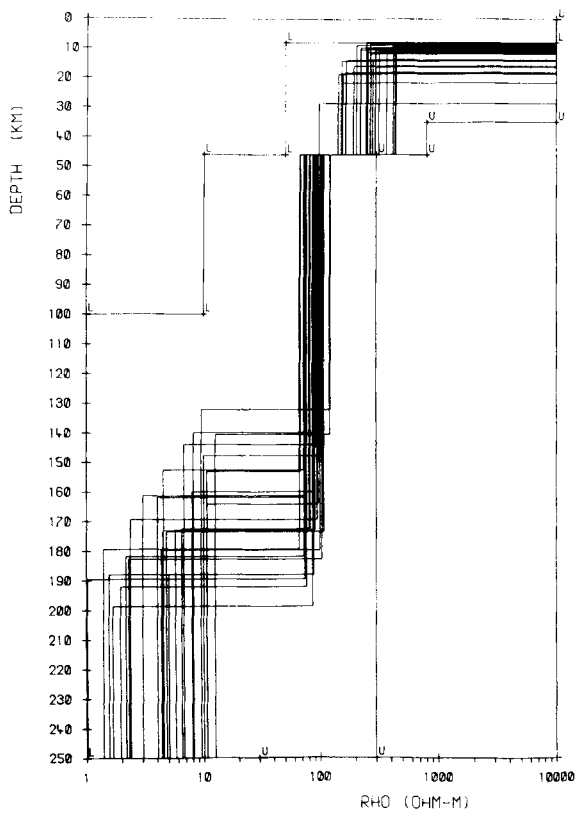

Figure 3. The resistivity profiles of those 4-layer models that are acceptable to all 18 80 per cent confidence intervals. The final bounds of the search procedure are again illustrated by L and U.

Downloaded from https://academic.oup.com/gji/article/68/2/371/692185 by guest on 20 April 2024

The system matrix **A**, as given by

$$\mathbf{\Delta c} = \mathbf{A} \cdot \mathbf{\Delta p} \tag{1}$$

where $\mathbf{\Delta p}$ is an n-length vector describing small order variations in the n model parameters $\mathbf{p}$, $\mathbf{\Delta c}$ is an m-length vector describing the changes introduced on the m observations of the variations $\mathbf{\Delta p}$, and $\mathbf{A}$, an $m \times n$ matrix relating $\mathbf{\Delta c}$ to $\mathbf{\Delta p}$ (note on notation, capital letters in bold-face type refer to matrices, small letters in bold-face type to vectors), represents a first-order Taylor series linearization of the functional relationship between the model parameters, $\mathbf{p}$, and the calculated values, $\mathbf{c}$. Matrix $\mathbf{A}$ consists of m rows, each row corresponding to the sensitivity of one observation to a variation in each of the n model parameters, and n columns, each column corresponding to the sensitivity of all m observations to one particular model parameter.

Because some observations are usually considered to be better estimated than others, it is essential that the system matrix be weighted to reflect the certainty of the individual observations. The weighting matrix commonly used is that given by the variance–covariance matrix of the data divided by the problem variance, i.e. $\mathbf{S} = \mathbf{V}/\sigma^2$ where $V_{ij} = E[\xi_i \xi_j]$, the expectation value of the covariance between the error in the ith observation and that in the jth observation, and σ^2 is the problem variance. The transformed system matrix $\mathbf{A}'$, given by $\mathbf{A}' = \mathbf{S}^{-1/2}\mathbf{A}$, describes the relationship between the transformed observations, $\mathbf{\Delta c}' = \mathbf{S}^{-1/2}\mathbf{\Delta c}$, all of variance σ^2, and the model parameters, i.e.

$$\mathbf{\Delta c}' = \mathbf{A}' \cdot \mathbf{\Delta p}. \tag{2}$$

An estimate of the problem variance for weighted least-squares problems, i.e. when the data do not all display the same individual variance, is given by

$$\hat{\sigma}^2 = \frac{(\mathbf{\Delta c})^t \mathbf{V}^{-1} \mathbf{\Delta c}}{m-n} \tag{3}$$

(Hamilton 1964, p. 130; Inman 1975).

As shown by Inman (1975), the covariance matrix of the model parameters is given by

$$\mathrm{cov}(\mathbf{p}) = \sigma^2 (\mathbf{A}^t \mathbf{V}^{-1} \mathbf{A})^{-1}, \tag{4}$$

and from this the correlation matrix of the model parameters, which indicates the interdependence between parameters, is derivable. The elements of the correlation matrix are given by

$$[\mathrm{cov}(\mathbf{p})]_{ij} = \frac{[\mathrm{cov}(\mathbf{p})]_{ij}}{[\mathrm{cov}(\mathbf{p})]_{ii}\,[\mathrm{cov}(\mathbf{p})]_{jj}}. \tag{5}$$

Wiggins (1972), and recently Edwards, Bailey & Garland (1980), detailed how the problem described by equation (2) may be reparameterized by a singular valve decomposition (SVD) of matrix $\mathbf{A}'$. Assuming that there exist k independent equations in (2), then matrix $\mathbf{A}'$ has rank k and can be factored as

$$\underset{m \times n}{\mathbf{A}'} = \underset{m \times k}{\mathbf{U}} \quad \underset{k \times k}{\mathbf{\Lambda}} \quad \underset{k \times n}{\mathbf{V}^t} \tag{6}$$

where $\mathbf{U}$ contains k eigenvectors $\mathbf{u}_i$ of length m associated with the observations, $\mathbf{\Lambda}$ is a diagonal matrix of k eigenvalues, λ_i, $\mathbf{V}$ contains k eigenvectors $\mathbf{v}_i$ of length n associated with the parameters, and k is the number of degrees of freedom, given by

$$k = \Sigma \lambda_i^2/(\lambda_i^2 + \sigma^2).$$

(Wiggins 1972).

Downloaded from https://academic.oup.com/gji/article/68/2/371/692185 by guest on 20 April 2024

Reparameterizing the data, $\Delta \mathbf{c}'$, and the model parameters, $\mathbf{p}$, by matrices $\mathbf{U}$ and $\mathbf{V}$ gives

$$\mathbf{c}^* = \mathbf{U}^t \, \mathbf{S}^{-1/2} \, \mathbf{c} \tag{7}$$

as eigendata, and

$$\mathbf{p}^* = \mathbf{V}^t \, \mathbf{p} \tag{8}$$

as eigenparameters (Edwards *et al.* 1980).

If $k < n$, then the complexity of the model cannot be resolved by the data set used, and hence either simpler models must be sought, or *a priori* information must be included.

The variance of each eigenparameter is given by

$$\text{var}(p_i^*) = [\sigma \lambda_i / (\lambda_i^2 + \sigma^2)]^2 \tag{9}$$

and the resolution matrix by

$$\mathbf{R} = \sum_j [\lambda_j^2 / (\lambda_j^2 + \sigma^2)] \, \mathbf{v}_j \, \mathbf{v}_j^t \tag{10}$$

3.2 APPLICATION

The available data set consists of estimates of apparent resistivity and phase, and their associated variances, at nine periods. Although it is well known that apparent resistivity and phase are not independent, and in fact for theoretical data the phase is related to the apparent resistivity by Hilbert transformation (Weidelt 1972; Fischer & Schnegg 1980) by including both data the space of acceptable solutions is reduced to that given by the overlap of the two individual spaces of acceptable solutions, i.e.

$$\mathbf{T} = \mathbf{R} \cap \mathbf{P},$$

where $\mathbf{T}$ is the set of solutions acceptable to both data, $\mathbf{R}$ is the set of solutions acceptable to the resistivity information, and $\mathbf{P}$ is the set of solutions acceptable to the phase information.

If the sets do not overlap, i.e. $\mathbf{R} \cap \mathbf{P} = 0$ (null set), then $\rho_a(T)$ and $\phi(T)$ are incompatible, or their variances have been underestimated, and no common model exists. If one set is totally contained by the other, i.e. $\mathbf{R} \subset \mathbf{P}$ or $\mathbf{P} \subset \mathbf{R}$, then the other set is redundant.

As was shown in Jones (1980), the real and imaginary parts of the estimated $C(\omega, 0)$ are fully compatible, and hence, because the Earth is a minimum phase system, ρ_a and ϕ illustrated in Fig. 1 are also compatible.

The data used for the study were not ρ_a and ϕ values, but $\log_{10} \rho_a$ and ϕ values, because ρ_a is approximately lognormally distributed, not normally distributed (Bentley 1973), for ϕ the difference between a normal distribution and its closest equivalents for data distributed on a circle, i.e. the wrapped normal and the von Mises distributions, was ignored (see Mardia 1972 pp. 68–69). In a similar manner, the model parameters were not the resistivities ρ_i, and thicknesses, h_i, of the model, but $\rho_i' = \log_{10}(\rho_i)$ and $h_i' = 2 \log_{10}(h_i)$, because, as has been stressed by Weidelt (1972), Loewenthal (1975) and others, the natural scales of the layer parameters are logarithmic. The layer parameter h_i' is twice the logarithm of h_i because of equal penetration depth arguments. If a layer of initial thickness h is halved in size, then its resistivity must be reduced to one-quarter, not one-half, of the initial value in order that the fields are attenuated to the same degree on passing through it. This is a direct consequence of the fact that the skin depth of a medium is not proportional to the resitivity of the medium, but to its square root.

The variance–covariance matrix $\mathbf{V}$ was assumed to be diagonal as the estimations of ρ_a and ϕ at different periods were not related, and hence their errors should not correlate. For

Downloaded from https://academic.oup.com/gji/article/68/2/371/692185 by guest on 20 April 2024

Table 2. Upper triangle: correlation matrix of the parameters of the 3-layer model specified in Table 1. Lower triangle: correlation matrix of the same model as for Table 2, but assuming that ρ'_1 is a problem constant and not a problem variable.

	ρ'_1	ρ'_2	ρ'_3	h'_1	h'_2
ρ'_1	100	59	−23	−94	84
ρ'_2		100	16	−81	46
ρ'_3		38	100	13	−59
h'_1		−90	−25	100	−84
h'_2		−8	−74	−10	100

apparent resistivity, the variances were determined on a logarithmic scale to be in accord with the assumption that ρ_a is lognormally distributed.

For the three-layer model detailed in Table 1, the SVD eigenvectors, $\mathbf{v}_i$, and their corresponding eigenvalues, λ_i are illustrated in Fig. 4, left side, together with the diagonal of the resolution matrix, given by equation (10), for the system matrix containing both $\log_{10}(\rho_a)$ and ϕ information. For the data and the model used, the best estimated parameter is h'_1. The fifth eigenvector has an eigenvalue of 0.02, which indicates that the data cannot resolve that eigenparameter, and, as can be seen in Fig. 4, left side, the fifth eigenvector comprises of almost solely $h'_2 = 2\log_{10}(h_2)$. The correlation matrix (Table 2, upper

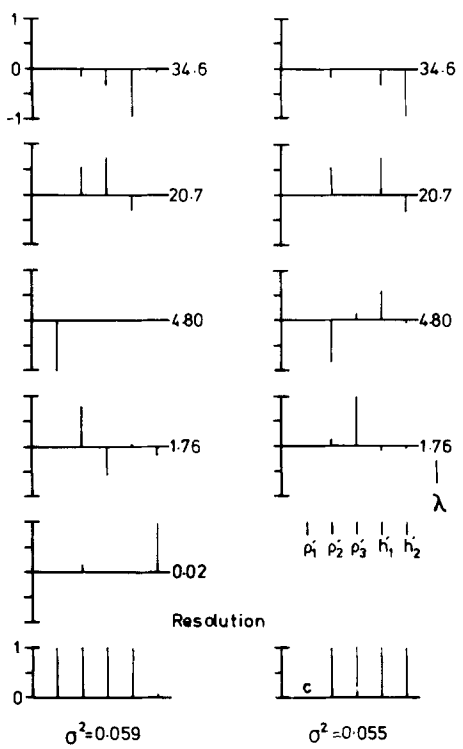

Figure 4. Left side: an SVD analysis of the best fitting 3-layer model detailed in Table 1. The eigenvectors are given in decreasing eigenvalue order, where the eigenvalues are as listed. The model parameters are in order of all layer resistivity parameters followed by layer thickness parameters, i.e. ρ'_1, ρ'_2, ρ'_3, h'_1 and h'_2. The main diagonal of the resolution matrix is illustrated at the bottom of the column, and the problem variance is given at the base of the column. Right side: an SVD analysis of the same model as for left side, but assuming that ρ'_1 is a problem constant and not a problem variable.

Downloaded from https://academic.oup.com/gji/article/68/2/371/692185 by guest on 20 April 2024

triangle) indicates, however, that although h'_2 cannot be resolved, its value has a great influence on the other parameters, especially ρ'_1 and h'_1. Hence, without any *a priori* information, the depth to the second interface is very badly determined. In the Monte-Carlo inversion undertaken in Section 2, ρ_1 was not considered a variable of the problem, but a constant with the value of $10^4\,\Omega$m. Repeating an SVD analysis of the data and the model, but assuming ρ'_1 is an *a priori* fact, therefore non-variable, results in the four eigenvectors as shown in Fig. 4, right side. From the diagonal of the resolution matrix (Fig. 4, right side, bottom), where '*c*' denotes a problem constant, it is clear that all the other four parameters are well resolved. Indeed, for this problem, h'_2 is the best resolved parameter, because eigenvector 1 consists of the terms $(-0.14)\,\rho'_2+(-0.30)\,h'_1+(-0.94)\,h'_2$. Eigenparameters 2 and 3 indicate that the two next best determined are ρ'_2 and h'_1, whilst the least well derived is ρ'_3. Parameters ρ'_2 and h'_1 show the largest intercorrelation (Table 2, lower triangle), with h'_2 and ρ'_3 next, the others are virtually uncorrelated. That Fig. 2 does not appear to agree totally with the SVD analysis (Fig. 4, right side), is due to the fact that the Monte-Carlo inversion was undertaken with the assumption that the problem variance was unity. As shown in Fig. 4, the actual problem variance is 0.055, which indicates that the internal consistency of the data is superior to the variances estimated. Hence it is justifiable to set the problem variance to 0.055 (Wiggins 1972) and repeat the Monte-Carlo inversion. This was not undertaken for the 3-layer model.

For the 4-layer best fitting model detailed in Table 1, an SVD analysis gave the eigeninformation illustrated in Fig. 5, and correlation matrices as given in Table 3. Fig. 5, left side, and Table 3, upper triangle are pertinent to the problem where all seven parameters $(\rho'_1, \rho'_2, \rho'_3, \rho'_4, h'_1, h'_2, h'_3)$ are assumed to be variables. The sixth and seventh eigenvectors and the resolution matrix diagonal (Fig. 5, left side), infer that the value of ρ'_1 cannot be resolved from the data set, that ρ'_2 is badly resolved, and that h'_1 is not well resolved. The best determined parameters is h'_2 (eigenvectors 1 and 2). The correlation matrix (Table 3, upper triangle) infers that the parameters are highly interdependent. With the *a priori* information that $\rho_1 = 10^4\,\Omega$m and $h_1+h_2=46$ km, an SVD analysis of the data with five problem variables, where h'_1 and h'_3 now strictly refer to the depths to the bottom of the layers, i.e. d'_1 and d'_3, yields the eigensolutions illustrated in Fig. 5, right side, with the associated parameter correlation matrix given in Table 3, lower triangle. For the problem, all parameters, with the exception of ρ'_4, are resolvable, and ρ'_4 is quite well resolved ($R_{44}=0.72$). The best determined parameters are h'_1 (strictly d'_1) and ρ'_3. The small value of problem variance, 0.036, again indicates that the data have a higher degree of internal consistency than is inferred by the estimated variances. Repeating the Monte-Carlo inversion of the data but for confidence intervals which are reduced by a factor of 0.316, i.e. the

Table 3. Upper triangle: as for Table 2 (upper triangle) for the 4-layer model detailed in Table 1. Lower triangle: correlation matrix for the same model as Table 3 (upper triangle), but assuming that ρ'_1 and d'_2, where $d'_i = 2\log_{10} d_i$ (depth to base of ith layer), are problem constants and not problem variables. Here h'_1 and h'_3 imply d'_1 and d'_3.

	ρ'_1	ρ'_2	ρ'_3	ρ'_4	h'_1	h'_2	h'_3
ρ'_1	100	−22	−30	−82	−01	38	−16
ρ'_2		100	93	21	−97	75	99
ρ'_3		−82	100	35	−86	54	93
ρ'_4		−21	36	100	−02	−33	13
h'_1		−98	72	18	100	−88	−97
h'_2						100	75
h'_3		34	−50	−80	−29		100

Downloaded from https://academic.oup.com/gji/article/68/2/371/692185 by guest on 20 April 2024

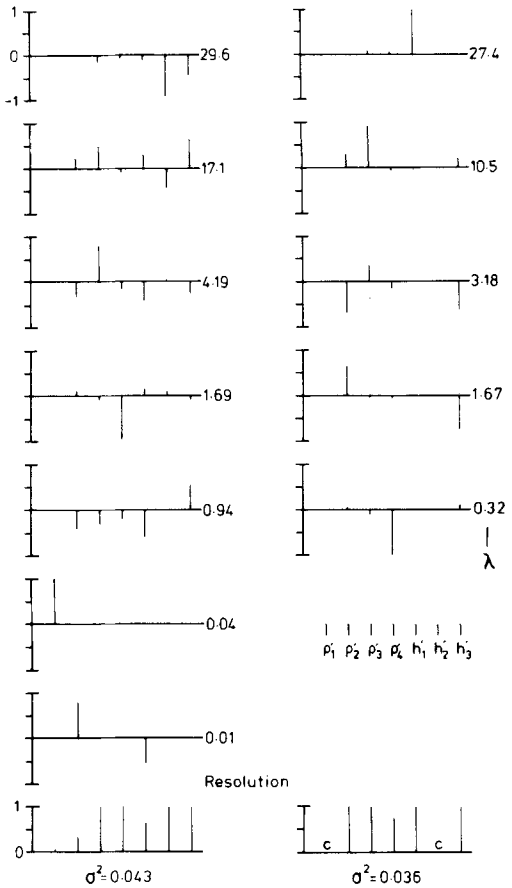

Figure 5. Left side: as for Fig. 4 (left side) for the 4-layer model detailed in Table 1. Right side: an SVD analysis of the same model as left side, but assuming that ρ'_1 and $d'_2 = 2\log_{10}(h_1 + h_2)$ are problem constants and not problem variables. Here h'_1 and h'_3 refer to the depths of the bottom of the layers, i.e. d'_1 and d'_3, and not the thicknesses of the layers.

square root of 0.10, yielded models, fitting to all 18 95 per cent confidence intervals, within the bounds illustrated in Fig. 6. Those models accepted, out of 10 000 tested, had parameters with standard deviations shown by the error bars in the figure, and the dashed line is the ρ–d profile of the best fitting model, as detailed in Table 1. Fig. 6 agrees with the SVD analysis as both infer that ρ'_3 and d'_1 are very well estimated, whilst ρ'_4 is worst estimated. The correlation matrix (Table 3, lower triangle) shows that d'_1 is highly correlated in an inverse manner to ρ'_2, which implies that equivalent models may be found by increasing d_1 and simultaneously decreasing ρ_2. This is illustrated by the best fitting model which displays virtually the minimum permitted value of d_1 and close to the maximum permitted value of ρ_2.

4 Implications to crust–mantle structure

The initial inversion of the data was undertaken to discover which 3-layer models, with $\rho_1 = 10^4\,\Omega$m, fit the data set. Examples of such acceptable models are illustrated in Fig. 2, and the best fitting solution discovered is given in Table 1. All models display a monotonically

Downloaded from https://academic.oup.com/gji/article/68/2/371/692185 by guest on 20 April 2024

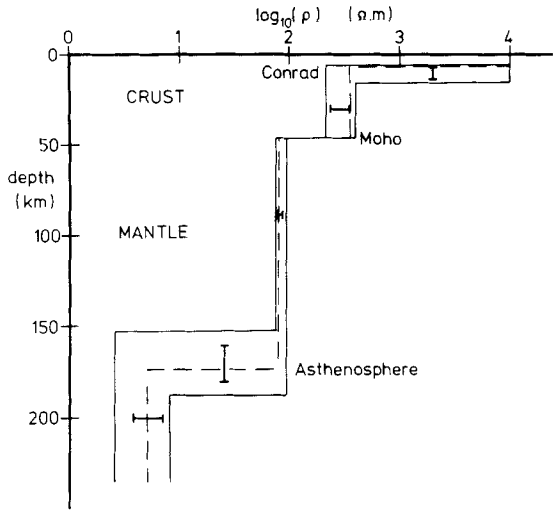

Figure 6. Solid lines: the bounds of those models acceptable to all 18 95 per cent confidence intervals of the reduced-variance data set. Dashed line: best fitting 4-layer model. Error bars: the ranges of 68 per cent of the acceptable model parameters.

increasing conductivity with depth, with a 'crust' of 10^4 Ωm which is 20–30 km thick, on a 'mantle' of 85–145 Ωm. Then, at a badly estimated depth of 130–190 km is a highly conducting layer of 2–15 Ωm.

In a recent paper however, Bungum, Pirhonen & Husebye (1980) derived a crustal thickness for the whole of the northern region of Fennoscandia of 45–47 km from seismic evidence. The most accurately determined parameter of the technique used (the spectral ratio method) is the depth to the Moho, crustal layering does not strongly affect this parameter. For the Kiruna station, Bungum *et al.* estimated a Moho depth of 45.5 ± 0.6 km standard deviation. In order to discover if this depth was compatible with the geomagnetic observations, the second Monte-Carlo inversion was undertaken, as described in Section 2, with an intracrustal discontinuity, of variable depth, to correspond to a Conrad seismic discontinuity. The inversion was constrained to give models with an interface at 46 km.

From the results of the inversion of the reduced variance data set (see Section 3.2), the acceptable models of which had bounds as illustrated in Fig. 6, five important points are noted:

(1) an intracrustal geoelectric boundary occurs at a depth of 6.5–16 km;
(2) the lower crustal layer has an intermediate resistivity, $\rho_2 = 215$–400 Ωm;
(3) there is not a large electrical resistivity contrast across the Moho;
(4) the upper mantle is moderately conductive, with $\rho_3 = 70$–95 Ωm; and
(5) there is a transition to a highly conducting layer, of $\rho_4 = 2.5$–8.1 Ωm, at a depth of 153–187 km.

Dealing with these points in order:

Point 1

The inferred intracrustal geoelectric boundary corresponds reasonably well with current best estimates of the thickness of the upper crust, from seismic studies, of 16 ± 4 km (Husebye 1980, private communication). Hence it may be the electrical equivalent of the seismic Conrad discontinuity.

Downloaded from https://academic.oup.com/gji/article/68/2/371/692185 by guest on 20 April 2024

Point 2

A lower crustal layer exhibiting such intermediate resistivities under a Precambrian shield region was shown by Jones (1981) to have counterparts on the eastern and southern edges of the Canadian shield. The layer is often correlatable with a seismic layer of transitional compressional wave velocity $V_p = 6.8–7.2\,\mathrm{km\,s^{-1}}$, and is of the Type II class as defined by Jones (1981). From an examination of the possible candidates for this layer, it was concluded that hydrous conditions must prevail and that an amphibolite displays the required characteristics.

Point 3

The electrical resistivity contrast across the Moho is, on a logarithmic scale, only a factor of about 1.2. Although an electrical boundary and an acoustic boundary are sometimes at the same depth (see, for example, Hutton, Ingham & Mbipom 1980), they are often not. For northern Sweden, Theilen & Meissner (1979) doubt that there is even a strong acoustic interface at the Moho – 'This fact (of weak P_mP arrivals) can well be explained by a positive velocity gradient within the crust leading to a small or even non-existent velocity step at the Moho.'

Point 4

Such a relatively conducting upper mantle under Precambrian regions is rather uncommon (see, for example, Jones 1981, figs 1 and 2), but an upper mantle of 40–60 Ωm as a global figure was interpreted by Schmucker (1974, reported in Haak 1980) for continental areas, from an analysis of S_q- and D_{st}-variations.

Point 5

The transition to a highly conducting layer of $\rho = 2.5–8.1\,\Omega\mathrm{m}$ at a depth of 153–187 km is well correlated with the depth of a low-velocity layer observed under the Baltic shield. This low compressional wave velocity layer, LV_pL, has been interpreted as existing between 170–190 km by Cassell & Fuchs (1979), between 150–250 km by Nolet (1977), and between 150–220 km by Given & Helmberger (1980). These results are to be contrasted by a figure of 250 km for the lithospheric thickness of the Baltic shield, as derived by Sacks, Snoke & Husebye (1979). The heat flow in northern Sweden is 40 ± 3 (standard deviation) $\mathrm{mW\,m^{-2}}$ (Eriksson & Malmqvist 1979, ignoring the anomalously high A_1 measurement), which, according to Chapman & Pollack (1977), should infer a lithosphere of greater than 200 km thickness. Exceptions to this rule have been illustrated by Ádám (1980), and are principally the Canadian shield (Wickens 1971; Wickens & Buchbinder 1980) and south-central USA (Biswas & Knopoff 1974), both of which exhibit low heat flow ($q \sim 40\,\mathrm{mW\,m^{-2}}$) with pronounced shear wave low-velocity layers in the upper mantle, LV_sL's, but without compressional wave low-velocity layers, LV_pL's. An empirical relationship given by Ádám (1978), for the depth to the Intermediate Conducting Layer (ICL), or asthenosphere, is $h_{\mathrm{ICL}} = 155\,q^{-1.46}$, where q is the heat flow in heat flow units. Substituting the figure for northern Sweden of $q = 0.96$ HFU, gives $h_{\mathrm{ICL}} = 164$ km, which agrees with the majority of the seismic investigations and also with the geomagnetic data. In contrast, an interpretation of the generalized curve for the East European platform shows no 'well-developed' electrical asthenosphere (Vanyan *et al.* 1977), where a 'well-developed' asthenosphere is defined by Vanyan *et al.* (1977) as exhibiting a conductance of greater than 1000 S, i.e. thickness × conductivity. The asthenosphere derived from this work has a minimum thickness of 60 km; any

Downloaded from https://academic.oup.com/gji/article/68/2/371/692185 by guest on 20 April 2024

thinner and its thickness would be resolvable, especially by the phase information (note: the comments by Vanyan *et al.* were made solely on the apparent resistivity information, no phase data were included). Hence this electrical asthenosphere is certainly 'well-developed' because it exhibits a minimum conductance of 12 000 S (60 000/5).

5 Possible geotherm under northern Sweden

The important role that could be played by geomagnetic studies, i.e. Geomagnetic Depth Soundings (GDS), Magnetotelluric investigations (MT), or application of the relatively new Horizontal Spatial Gradient method (HSG – see, for example, Jones 1980), in helping to understand the dynamic processes involved in mantle convection and magma migration has been stressed by many workers, most recently by Waff (1980). This is because of all lithological parameters that are temperature-dependent, electrical conductivity is one of the most sensitive to thermal variation. Thus, regional electrical conductivity profiles deduced from one, or more, of the above techniques, combined with laboratory data detailing the electrical properties of probable mantle materials at mantle temperatures (the effect of pressure, beyond that required to produce crack closure, is not considered to be important (see, for example, Duba 1976; Volarovich & Parkhomenko 1976), unless the depths are such that phase transitions may be involved), provide an important constraint on the mantle geotherm for the region.

Considering solid olivine, the lower limit on the conductivity–temperature relationship is taken from the measurements of Duba, Heard & Schock (1974), whilst the actual conductivity for olivine is believed by Shankland & Waff (1977) to be no greater than ten times Duba *et al.*'s results. Taking Duba *et al.*'s data, and the ρ^*–z^* inversion (Schmucker 1970) of the geomagnetic data (illustrated in Fig. 7), yields the olivine geotherm marked DHS in Fig. 7. The lower limit is given by adopting Shankland & Waff's (1977) suggestion of ten times the conductivity relationship of Duba *et al.*, to yield geotherm RSP × 10 in Fig. 7. Possible geotherms from solid ultramafic rocks are derived from Rai & Manghnani's (1978) studies. The lower and upper geotherms (marked 'l' and 'u') are deduced for a garnet lherzolite and a spinel lherzolite respectively, where the former should be more representative of a continental upper mantle and the latter of an oceanic upper mantle. These two are in fact also the bounds of the various rock types studied by Rai & Manghnani (1978). The shaded region in Fig. 7 are the bounds deduced from taking the ρ^*–z^* inversion coupled with Rai & Manghnani's data.

These geotherms may be compared with published geotherms; Ringwood's continental geotherm (Clark & Ringwood 1964; Ringwood 1975), Tozer's continental geotherm (Tozer 1967), Hall's Canadian shield temperature–depth relationship (Hall 1977), and Anderson's dry garnet lherzolite geotherm (Anderson 1980). If there is a slight partial melt, which should be expected in an asthenosphere, then the 'hump' on Anderson's geotherm will reduce slightly to a maximum value of 1450°C. All geotherms in Fig. 7, with the exception of DHS, are below the dry lherzolite solidus and the dry basalt solidus (see Anderson 1980).

The existence of the seismically observed asthenosphere requires a 1–3 per cent melt fraction of the rock to give the reduced seismic velocities (see, for example, Stocker & Gordon 1975). For a 2 per cent melt fraction at a pressure of 50 kbar, an effective conductivity of 0.2 S m^{-1} (i.e. the conductivity of the highly conducting layer) infers a temperature of 1500°C, from the effective medium theory of Shankland & Waff (1977) as applied to their basalt melt conductivity and the RSP × 10 olivine conductivity data. The solid triangle indicates a 3 per cent melt if the more resistive DHS olivine conductivity data are used. A 3 per cent melt of RSP × 10 olivine at 50 kbar, giving an effective conductivity of

Downloaded from https://academic.oup.com/gji/article/68/2/371/692185 by guest on 20 April 2024

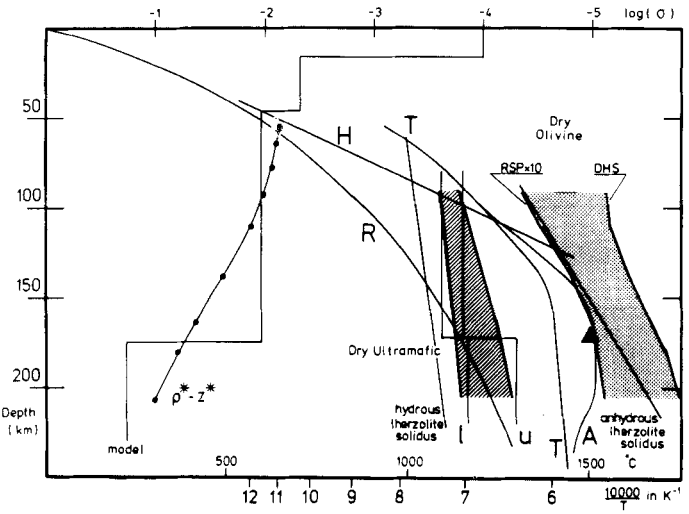

Figure 7. Model: The best-fitting 4-layer solution, as detailed in Table 1; ρ^*–z^*: the Schmucker ρ^*–z^* inversion of the data; R: Ringwood's Precambrian geotherm (Clark & Ringwood 1964); T: Tozer's Precambrian geotherm (Tozer 1967); H: Hall's Canadian shield temperature–depth relationship (Hall 1977); A: Anderson's dry garnet lherzolite geotherm (Anderson 1980); hydrous and anhydrous lherzolite solidii: of Kushiro *et al.* (1968); DHS: solid dry olivine temperatures as inferred from the ρ^*–z^* inversion and the laboratory data of Duba *et al.* (1974) at atmospheric pressure; RSP×10: the solid dry olivine temperatures as inferred from the ρ^*–z^* inversion and the upper limit conductivity–temperature relationship, suggested by Shankland & Waff (1977), at atmosphere pressure; Shaded area: dry ultramafic temperatures as inferred from the ρ^*–z^* inversion and the laboratory data of Rai & Manghnani (1978). The colder bound is for garnet lherzolite, and the hotter bound is for spinel lherzolite, both at atmospheric pressure; l: the lower bound ultramafic temperature as inferred from the best fitting model and the garnet lherzolite data of Rai & Manghnani (1978), at atmospheric pressure; u: the upper bound ultramafic temperature as inferred from the best fitting model and the spinel lherzolite data of Rai & Manghnani (1978), at atmospheric pressure; Solid triangle: the inferred temperature of a 2 per cent melt fraction of RSP×10 olivine, or a 3 per cent melt fraction of DHS olivine, at 50 kbar pressure, from the effective medium theory of Shankland & Waff (1977). This point may be regarded as the upper bound of the temperature of the asthenospheric zone under the Fennoscandian shield.

0.2 S m^{-1}, would infer a temperature of 1425°C. Hence, a partial melt of the order of 3 per cent infers a temperature value at a depth of 170 km which lies between the geotherms proposed by Tozer and Anderson, assuming that Shankland & Waff's effective medium theory is valid and that the solid conductivities given by either of the curves DHS or RSP × 10 are valid.

However, if there should exist free water at these depths, then the proposed temperatures are well above the hydrous lherzolite solidus of Kushiro, Syono & Akimoto (1968). This solidus is applicable when the hydrostatic pressure equals the lithostatic pressure, and should this condition not be met, the true solidus will lie between the hydrous and anhydrous solidii indicated in Fig. 7. Too little is known of the conductivity variation with temperature of rocks, which can be considered to represent mantle constituents, under hydrous mantle conditions to be able to even estimate the effects introduced. It is possible, however, that under hydrous conditions the temperatures could be as low as the hydrous lherzolite solidus proposed by Kushiro *et al.* (1968).

Conclusions

The inversion of the $\hat{C}(\omega, 0)$ data from northern Sweden, as detailed in Jones (1980), by a

Downloaded from https://academic.oup.com/gji/article/68/2/371/692185 by guest on 20 April 2024

refined version of the Monte-Carlo random model parameter choice procedure (Jones & Hutton 1979), illustrated that 3- and 4-layer models could be found which satisfied all 18 80 per cent confidence intervals. The acceptable models, illustrated in Figs 2 and 3, all display a moderately resistive lower crust and upper mantle, underlain by a good conducting zone beginning at an ill-defined depth of 130–190 km.

An analysis of the system matrix of the best fitting models illustrated how important was the *a priori* knowledge given by the AMT information of Westerlund (1972), of a top layer of resistivity $10^4\,\Omega$m. This resistivity could not be resolved by the 4-layer best fitting model, and its introduction as a problem constant rather than a problem variable led, in both the 3- and the 4-layer solutions, to correlation matrices exhibiting a lesser degree of model parameter intercorrelations. The analysis showed that the deep highly conducting layer is well resolved by the data, and is not an artifact of the modelling procedure used. The problem variances indicated that the data set have a higher internal consistency than that described by the estimated data variances. On reducing the data variances by a factor of 10, which is in fact a conservative value as the problem variance inferred a reduction by a factor of 20 was appropriate, those models acceptable to the variance-reduced 95 per cent confidence intervals had bounds as illustrated in Fig. 6.

The two major geophysical implications from this study are that there is not a strong, if any, resistivity contrast across the Moho, and that there is an electrical asthenosphere, of minimum thickness 60 km, beginning at 150–190 km depth. Both of these factors appear to have their counterparts in the various seismic models of the Baltic shield, with the comment by Theilen & Meissner (1979) that the Moho under northern Sweden is not a strong acoustic interface, and the interpretation of Nolet (1977), Cassell & Fuchs (1979) and Given & Helmburger (1980) of a compressional wave low-velocity layer, LV_pL, with its top interface somewhere between 150–170 km. That an asthenosphere is observed under a shield region may be due to the fact that the geomagnetic investigations, and the majority of the seismic investigations, were undertaken near to the edge of the shield, i.e. at Kiruna in the former case, and the Blue Road seismic project data (Cassell & Fuchs 1979) and the NORSAR array data (Given & Helmburger 1980) in the latter case. This must be contrasted with the East European platform which does not display an electrical asthenosphere (Vanyan *et al.* 1977). However Patton (1980), in an analysis of data from the 'Northern Platforms and Shields', which included the East European platform, the Baltic shield, Greenland and part of the Canadian shield, concluded that there must exist a shear wave low-velocity layer, LV_sL, between 80–250 km depth underlying the whole region. It may be significant that under the Canadian shield there is an LV_sL from 125–275 km, without a corresponding LV_pL (Wickens 1971; Wickens & Buchbinder 1980), whilst Reddy & Rankin (1971) report that there must be no large variation from a resistivity of 3500 Ωm in the upper mantle. At Reddy & Rankin's (1971) longest period, ~ 500 s, the skin depth for a 3500 Ωm layer is over 600 km, which implies that there cannot be an electrical asthenosphere under the central Canadian shield, Hence, under the Canadian shield and the East European platform there exist LV_sL's, without corresponding LV_pL's, or electrical asthenospheres, whilst under the Baltic shield there exists both an LV_pL and an electrical asthenosphere.

In attempting to derive a geotherm from the geoelectrical model and petrological information, it is glaringly obvious that insufficient information is known about the probable conditions in an asthenospheric layer. For solid crystalline olivine, the olivine geotherms for atmospheric pressure indicated by DHS and RSP × 10 (Duba *et al.* 1974; Shankland & Waff 1977) and the stippled area in between (Fig. 7), are inferred by the data. Curve RSP × 10 seems to be in accord with the relatively new dry garnet lherzolite geotherm

Downloaded from https://academic.oup.com/gji/article/68/2/371/692185 by guest on 20 April 2024

of Anderson (1980), and lies below the anhydrous lherzolite solidus. Alternatively, the data on solid ultramafic rocks of Rai & Manghnani (1977), where the lower and the upper bounds ('l' and 'u' respectively in Fig. 7) are for garnet and spinel lherzolite, and the shaded region is that for the ρ^*-z^* inversion, infer a much colder mantle with a temperature at 100 km in accord with Tozer's (1967), Hall's (1977) and Anderson's (1980) geotherms, but which has a very small gradient thus approaching Ringwood's geotherm (Clark & Ringwood 1964) at 150–200 km depth. However, the existence of a seismic LV_pL implies a small fraction of partial melt. The triangle in Fig. 7 is for either a 2 per cent melt of RSP × 10 olivine, or a 3 per cent melt of DHS olivine, at 50 kbar, as extrapolated from the factors given by Shankland & Waff (1977), with the assumption that the pressure effect on the basalt melt is zero, i.e. $\Delta V_m = 0$ in equation (1) of Shankland & Waff. A small partial melt in a mix of Rai & Manghnani's solid garnet lherzolite and a basalt melt would not reduce the geotherm much below that marked 'l', or the colder bound of the shaded region. If there should be free water present, however, all these geotherms are above Kushiro *et al.*'s (1968) hydrous lherzolite solidus, hence much greater fractions of partial melt may be present inferring a colder mantle at 150–200 km depth.

In conclusion, until more is known of the conditions within as asthenospheric layer, the temperature point indicated by the triangle can be considered an upper bound, with a probable lower bound being indicated by the hydrous lherzolite solidus.

Acknowledgement

The author wishes to thank the Deutsche Forschungsgemeinschaft for financial support.

References

Ádám, A., 1978. Geothermal effects in the formation of electrically conducting zones and temperature distribution in the Earth, *Phys. Earth planet. Int.*, **17**, P21–P28.

Ádám, A., 1980. Relation of mantle conductivity to physical conditions in the asthenosphere, *Geophys. Surv.*, **4**, 43–69.

Anderson, O. L., 1980. The temperature profile of the upper mantle, *J. geophys. Res.*, **85**, 7003–7010.

Bentley, C. R., 1973. Error estimation in two-dimensional magnetotelluric analyses, *Phys. Earth planet. Int.*, **7**, 423–430.

Biswas, N. N. & Knopoff, L., 1974. The structure of the upper mantle under the United States from the dispersion of Rayleigh waves, *Geophys. J. R. astr. Soc.*, **36**, 515–539.

Bungum, H., Pirhonen, S. E. & Husebye, E. S., 1980. Crustal thickness in Fennoscandia, *Geophys. J. R. astr. Soc.*, **63**, 759–774.

Cassell, B. R. & Fuchs, K., 1979. Seismic investigations of the subcrustal lithosphere beneath Fennoscandia, *J. Geophys.*, **46**, 369–384.

Chapman, D. S. & Pollack, H. N., 1977. Regional geotherms and lithospheric thickness, *Geology*, **5**, 256–268.

Clark, S. P. & Ringwood, A. E., 1964. Density distribution and constitution of the mantle, *Rev. Geophys. Space Phys.*, **2**, 35–88.

Duba, A., 1976. Are laboratory electrical conductivity data relevant to the Earth?, *Acta Geodaet., Geophys. Montanist. Acad. Sci. Hung.*, **11**, 485–495.

Duba, A. G., Heard, H. C. & Schock, R. N., 1974. Electrical conductivity of olivine at high pressures and under controlled oxygen fugacity, *J. geophys. Res.*, **79**, 1667–1673.

Edwards, R. N., Bailey, R. C. & Garland, G. D., 1980. Crustal and upper mantle conductivity studies with natural and artificial sources, in *The Continental Crust and its Mineral Deposits*, ed. Strangway, D. W., *Spec. Pap. geol. Ass. Can., 20.*

Eriksson, K. G. & Malmqvist, D., 1979. A review of the past and present investigations of heat flow in Sweden, in *Terrestrial Heat Flow in Europe*, pp. 267–277, ed. Čermák, V. & Ryback, L., *Inter-Union Comm. of Geodyn. Sci. Rep. No. 58*, Springer-Verlag, Berlin.

Downloaded from https://academic.oup.com/gji/article/68/2/371/692185 by guest on 20 April 2024

Fischer, G. & Schnegg, P.-A., 1980. The dispersion relations of the magnetotelluric response and their incidence on the inversion problem, *Geophys. J. R. astr. Soc.*, **62**, 661–673.

Given, J. W. & Helmberger, D. V., 1980. Upper mantle structure of northwestern Europe, *J. geophys. Res.*, **85**, 7183–7194.

Gough, D. I. & Reitzel, J. S., 1967. A portable three component magnetic variometer, *J. Geomagn. Geoelectr.*, **19**, 203–215.

Haak, V., 1980. Relations between electrical conductivity and the petrological parameters of the crust and upper mantle, *Geophys. Surv.*, **4**, 57–69.

Hall, D, H., 1977. Partial melting and mineral-stability boundaries and their bearing on the seismic exploration of the lithosphere in Canada, *Can. J. Earth Sci.*, **14**, 2638–2650.

Hamilton, W. C., 1964. *Statistics in Physical Sciences, Estimation, Hypothesis Testing, and Least Squares*, Ronald Press Co., New York.

Hutton, V. R. S., Ingham, M. R. & Mbipom, E. W., 1980. An electrical model of the crust and upper mantle in Scotland, *Nature*, **287**, 30–33.

Inman, J. R., 1975. Resistivity inversion with ridge regression, *Geophysics*, **40**, 798–817.

Jones, A. G., 1977. Geomagnetic induction studies in S. Scotland, *PhD thesis*, University of Edinburgh.

Jones, A. G., 1980. Geomagnetic induction studies in Scandinavia – I. Determination of the inductive response function from the magnetometer array data, *J. Geophys.*, **48**, 181–194.

Jones, A. G., 1981. On a type classification of lower crustal layers under Precambrian regions, *J. Geophys.*, **49**, 226–233.

Jones, A. G. & Hutton, R., 1979. A multi-station magnetotelluric study in southern Scotland – II. Monte-Carlo inversion of the data and its geophysical and tectonic implications, *Geophys. J. R. astr. Soc.*, **56**, 351–368.

Keilis-Borok, V. I. & Yanovskaya, T. B., 1967. Inverse problems of seismology (structural review), *Geophys. J. R. astr. Soc.*, **13**, 223–234.

Kushiro, I., Syono, Y. & Akimoto, S.-I., 1968. Melting of a peridotite nodule at high pressures and high water pressures, *J. geophys. Res.*, **73**, 6023–6029.

Küppers, F. & Post, H., 1981. A second generation Gough-Reitzel magnetometer, *J. Geomagn. Geoelectr.*, **33**, 225–237.

Loewenthal, D., 1975. Theoretical uniqueness of the magnetotelluric inverse problem for equal penetration discretizable models, *Geophys. J. R. astr. Soc.*, **43**, 897–903.

Mardia, K. V., 1972. *Statistics of Directional Data*, Academic Press, New York.

Nolet, G., 1977. The upper mantle under western Europe inferred from the dispersion of Rayleigh modes, *J. Geophys.*, **43**, 265–285.

Patton, H., 1980. Crust and upper mantle structure of the Eurasian continent from the phase velocity and Q of surface waves, *Rev. Geophys. Space Phys.*, **18**, 605–625.

Price, A. T., 1962. The theory of magnetotelluric fields when the source field is considered, *J. geophys. Res.*, **67**, 1907–1918.

Rai, C. S. & Manghnani, M. H., 1978. Electrical conductivity of ultramafic rocks to 1820 Kelvin, *Phys. Earth planet. Int.*, **17**, 6–13.

Reddy, I. K. & Rankin, D., 1971. Magnetotelluric measurements in central Alberta, *Geophysics*, **36**, 739–753.

Ringwood, A. E., 1975. *Composition and Petrology of the Earth's Mantle*, McGraw-Hill, New York.

Sacks, I. S., Snoke, J. A. & Husebye, E. S., 1979. Lithosphere thickness beneath the Baltic shield, *Tectonophys.*, **56**, 101–110.

Schmucker, U., 1970. Anomalies of geomagnetic variations in the southwestern United States, *Bull. Scripps Inst. Oceanogr.*, **13**.

Schmucker, U., 1974. Erdmagnetische Tiefensondierung mit langperiodischen Variationen, presented at the *'Erdmagnetische Tiefensondierung'* Colloquium, Grafrath, Bavaria, Federal Republic of Germany, March 11–13.

Schmucker, U. & Weidelt, P., 1975. *Electromagnetic Induction in the Earth*, Lecture Notes, Aarhus University.

Shankland, T. J. & Waff, H. S., 1977. Partial melting and electrical conductivity anomalies in the upper mantle, *J. geophys. Res.*, **82**, 5409–5417.

Stocker, R. L. & Gordon, R. B., 1975. Velocity and internal friction in partial melts, *J. geophys. Res.*, **80**, 4828–4836.

Theilen, Fr. & Meissner, R., 1979. A comparison of crustal and upper mantle features in Fennoscandia and the Rhenish shield, two areas of recent uplift, *Tectonophys.*, **61**, 227–242.

Downloaded from https://academic.oup.com/gji/article/68/2/371/692185 by guest on 20 April 2024

Tozer, D. C., 1967. Towards a theory of thermal convection in the mantle, in *The Earth's Mantle*, pp. 325–353, ed. Gaskell, T. F., Academic Press, London.

Vanyan, L. L., Berdichewsky, M. N., Fainberg, E. B. & Fiskina, M. V., 1977. The study of the asthenosphere of the East European platform by electromagnetic sounding, *Phys. Earth planet. Int.*, **14**, P1–P2.

Volarovich, M. P. & Parkhomenko, E. I., 1976. Electrical properties of rocks at high temperatures and pressures, in *Geoelectric and Geothermal Studies (East-Central Europe, Soviet Asia)*, pp.319–369, ed. Ádám, A., *KAPG Geophys. Monogr.*, Akadémi ai Kiadó, Budapest.

Waff, H. S., 1980. Relations of electrical conductivity to physical conditions within the asthenosphere, *Geophys. Surv.*, **4**, 31–41.

Weidelt, P., 1972. The inverse problem of geomagnetic induction, *J. Geophys.*, **38**, 257–289.

Westerlund, S., 1972. Magnetotelluric experiments in the frequency range 0.01 Hz to 10 kHz, *KGO Rep. No. 72:10*, Kiruna Geophysical Observatory, November.

Wickens, A. J., 1971. Variations in lithospheric thicknesses in Canada, *Can. J. Earth Sci.*, **8**, 1154–1162.

Wickens, A. J. & Buchbinder, G. G. R., 1980. S-wave residuals in Canada, *Bull. seism. Soc. Am.*, **70**, 809–822.

Wiggins, R. A., 1972. The general linear inverse problem: Implications of surface waves and free oscillations for Earth structure, *Rev. Geophys. Space Phys.*, **10**, 251–285.

Downloaded from https://academic.oup.com/gji/article/68/2/371/692185 by guest on 20 April 2024